The effect of solvent on molar refraction and polarizability constant of heterocyclic drugs.

Swati Kolhe[1*], Dipak Patil[2], Avinash Sonar[3]

1*, 2 Sardar Vallabhbhai Patel Arts and Science College, Ainpur, Dist. Jalgaon (M.S.) India,

3. V. S. Naik Arts, Commerce and Science College, Raver, Dist. Jalgaon (M.S.) India.

E-mail: swatikolhe3@gmail.com

Mobile no. 9763241548

Abstract

Molar refraction (Rm) and polarizability constant (α) of heterocyclic drugs (Lamivudine, Simvastatin) in different solvents like acetone, methanol, ethanol, chloroform, dioxane and carbon tetrachloride were computed from experimental density (d) and refractive index (n) data at 303.15 K. Enhancement in overall polarizability of drug solution with relative drug concentration in each solvent and strong drug-solvent interaction due to perturbation in structural orientation of drug in different solvent has been observed.

Keywords

Lamivudine, Simvastatin, refractive index, density, molar refractivities and molar polarizability constant.

Introduction

The refractive index is an important additive property of liquid. It depends on the structural arrangement of atom in molecule and ionic strength of solution[1]. The value of refractive index depends upon the temperature[2] as well as the wavelength of light used. The properties of liquid such as viscosity, refractive index and ultrasonic velocity of binary mixtures are studied by many workers[3-7]. The study of refractive indices in mixed solvent is important as it gives information about solute solvent interactions[8-11]. The researcher gives more value to study additive properties such as molar refractivity and molar polarizability constant of different drugs[12-15]. The refractive index depends on the temperature and wave length of light. The extent

of refraction depends on –i) The relative concentration of atom or molecule ii) The structure of atom or molecule.[16]

Drug-solvent interactions are of great interest in chemical and pharmaceutical sciences. Molar refractivity data provides valuable information on electronic polarizability of individual ions in solution[17]. Studies based on refractive index measurements are used as an important tool for understanding molecular interactions in solution[18-20]. Different interactions in solution govern the pharmacokinetics and pharmacodynamics of drug. 4-amino-5- chloro-N-(2-(diethylamino) ethyl)-2 methoxybenzamide hydrochloride hydrate (Metoclopramide hydrochloride monohydrate) drug is a centrally acting anti-emetic, stimulating the motility of upper gastrointestinal tract and having parasympathomimetic activity[21].

In present work an effort has been made here to study molar refractivity and polarizability of Lamivudine and different solvents like Simvastatin in ethanol, methanol, chloroform, acetone, dioxane and carbon tetrachloride at 303.15 K.

Materials and method

In the present work the refractive indices of solvent and solutions were measured by Abbe's refractometer (±0.001). Initially, the refractometer was calibrated with glass piece (n=1.5220) provided with the instrument. The heterocyclic drugs were purchased from local retail pharmacy shop. Drug solutions of different concentrations were prepared (grinded tablets with a smooth pestle and mortar) in different solvents (AR grade) for evaluation of the molar refraction and polarizability constant. The temperature was maintained by using the thermostat. The data obtained was used to compute intermolecular interactions. The refractometric readings were taken as described in literature[22].

Theoretical Calculations

The molar refraction of solvent and solution are determined by using Lorentz-Lorentz equation.

$$Rm = \frac{(n^2-1)}{(n^2+2)} * \frac{M}{d} \quad (1)$$

$$Rm = \frac{4}{3}\pi N\alpha \quad (2)$$

$$Rm = X_1 R_{m1} + X_2 R_{m2} \quad (3)$$

where,

n - Refractive index of solution d - Density of solution

M - Molecular weight of solute Rm – Molar refraction

N - Avogadro's number ∝- Molar polarizability constant

X_1 and X_2 Mole fraction of solvent and solute in solution

The molar refraction of solute can be calculated as –

$$R_{m(solute)} = R_{m(solution)} - R_{m(solvent)} \quad (4)$$

The calculated value of molar refraction and molar polarizability constant of drugs with different concentration in different solvents are reported in Table 1.

Results and Discussion

The value of molar refraction (Rm) and polarizability constant (α) of polar solvents like, acetone, methanol and ethanol are found to be greater than non-polar solvents like chloroform, dioxane and carbon tetrachloride because polar solvent forms hydrogen bonding and may form complex with solute but non-polar solvent does not form hydrogen bonding and does not form complex with solute.

This may be characteristics to the fact that the dipole in the compound lies perpendicular to the longer axis of the molecule, which shows intermolecular attraction. This will be accompanied by increase in the value of molar refraction and molar polarizability constant with increasing concentration of solution because of mutual compensation of dipoles.

It could be seen that from table-1 and 2, the values of refractive index decrease with decrease in concentration of solution. As the concentration of solute decreases, distance between the molecules of solute increases, hence refractive index, molar refraction and polarizability constant of drugs decreases. The plot of molar refraction in different solvents with different concentration is shown in fig.1.

Table 1-: Refractive index (n), Density (d), Molar Refraction (Rm) and Polarizability constant (α) of Lamivudine in different solvent at 303.15K.

Conc. (mole/lit.)	Refractive index (n)	Density (gm/cm^3)	$Rm * 10^3$ $cm^3/mole$	$\propto * 10^{-26}$ cm^3
Acetone				
0.01	1.412	0.6343	0.08991	3.56
0.005	1.407	0.6299	0.08957	3.55
0.0025	1.402	0.6263	0.08911	3.53
0.00125	1.398	0.6220	0.08894	3.52
0.000625	1.394	0.6183	0.08867	3.51
Methanol				
0.01	1.442	0.7204	0.08418	3.34
0.005	1.436	0.7161	0.08369	3.32
0.0025	1.431	0.7118	0.08335	3.30
0.00125	1.427	0.7081	0.08311	3.29
0.000625	1.422	0.7038	0.08276	3.28
Ethanol				
0.01	1.498	0.9992	0.06724	2.66
0.005	1.493	0.9949	0.06695	2.65
0.0025	1.486	0.9898	0.06648	2.63
0.00125	1.481	0.9855	0.06619	2.62
0.000625	1.474	0.9804	0.06570	2.60
Chloroform				
0.01	1.333	0.7204	0.06544	2.59
0.005	1.329	0.7154	0.06518	2.58
0.0025	1.325	0.7118	0.06479	2.57
0.00125	1.320	0.7067	0.06434	2.55
0.000625	1.315	0.7016	0.06388	2.53
Dioxane				
0.01	1.409	0.9963	0.05688	2.25
0.005	1.403	0.9934	0.05630	2.23
0.0025	1.396	0.9905	0.05560	2.20
0.00125	1.391	0.9869	0.05518	2.19
0.000625	1.387	0.9840	0.05484	2.17

Carbon tetrachloride				
0.01	1.412	1.0253	0.05562	2.20
0.005	1.408	1.0224	0.05530	2.19
0.0025	1.403	1.0195	0.05486	2.17
0.00125	1.397	1.0159	0.05433	2.15
0.000625	1.391	1.0123	0.05379	2.13

Table 2-: Refractive index (n), Density (d), Molar Refraction (Rm) and Polarizability constant (α) of Simvastatin in different solvent at 303.15K.

Conc. (mole/lit.)	Refractive index (n)	Density (gm/cm^3)	$Rm * 10^3$ cm^3/mole	$\propto * 10^{-26}$ cm^3
Acetone				
0.01	1.369	0.6335	0.14906	5.91
0.005	1.366	0.6314	0.14847	5.88
0.0025	1.362	0.6285	0.14769	5.85
0.00125	1.359	0.6256	0.14727	5.83
0.000625	1.356	0.6234	0.14668	5.81
Methanol				
0.01	1.407	0.7929	0.12993	5.15
0.005	1.395	0.7748	0.12949	5.13
0.0025	1.381	0.7523	0.12916	5.12
0.00125	1.374	0.7407	0.12903	5.11
0.000625	1.365	0.7277	0.12850	5.09
Ethanol				
0.01	1.465	0.9485	0.12198	4.83
0.005	1.461	0.9449	0.12153	4.82
0.0025	1.458	0.9406	0.12140	4.81
0.00125	1.453	0.9362	0.12082	4.79
0.000625	1.449	0.9319	0.12045	4.77
Chloroform				
0.01	1.335	0.7270	0.11905	4.72
0.005	1.332	0.7233	0.11869	4.70
0.0025	1.328	0.7190	0.11809	4.68
0.00125	1.325	0.7154	0.11770	4.66
0.000625	1.321	0.7103	0.11721	4.64
Dioxane				
0.01	1.408	0.9942	0.10385	4.11
0.005	1.405	0.9905	0.10356	4.10
0.0025	1.402	0.9876	0.10318	4.09
0.00125	1.398	0.9847	0.10258	4.06
0.000625	1.394	0.9818	0.10196	4.04
Carbon tetrachloride				

0.01	1.406	1.0224	0.10054	3.98
0.005	1.402	1.0195	0.09995	3.96
0.0025	1.399	1.0166	0.09958	3.95
0.00125	1.395	1.0130	0.09904	3.92
0.000625	1.392	1.0094	0.09873	3.91

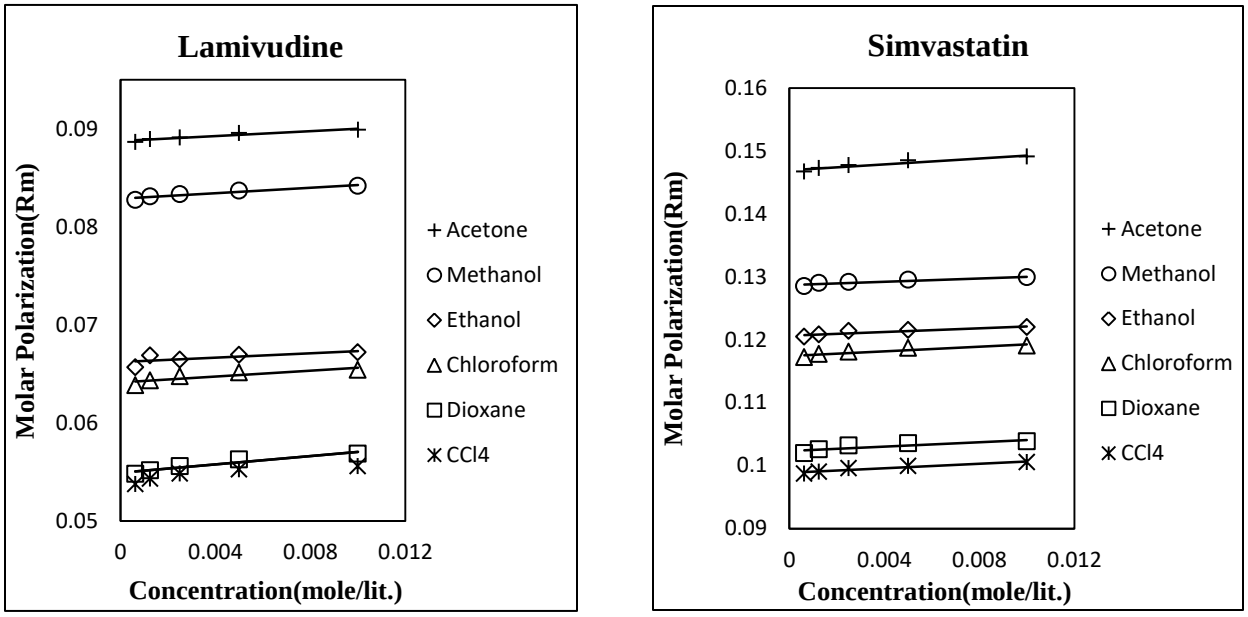

Figure 1. Molar refraction Vs drug concentration of drugs in different solvents at 303.15 K.

Conclusion

It is concluded that density and refractive index are strongly dependent on concentration. The increase in densities with concentration may be due to strengthening of solute-solvent interactions. Molar refraction shows linear relationship with concentration. Molar refraction (Rm) and polarizability constant (α)increases with polarity of solvent. The drug-solvent molecular interactions with different structural modification in different solvents have been observed. The polarizability constant is increased with drug concentration in all solvents due to increase in polarization of drug in solution; it shows strong solute – solvent interaction.

References

1. S. D. Thakur, D. T. Mahajan, Munot K. P., *Der Pharma Chemica*, 2011, 3(6), 165

2. M. R. Gaware "Studies of molar refraction and polarizability constant of 6-(4-chlorophenyl)-1, 2, 3, 4-tetrahydro-2, 4-dioxopyrimidine-5-carbonitrile in 60% DMSO in the temperature range 298 to 313 K." *Indian Journal of Science and Technology* 14.2 (2021):)113-118. https://doi.org/10.17485/IJST/v14i2.2118
3. D. T. Tayade, A. M. Kshirsagar, *The open physical chemistry Journal*, 2014, 6, 1. http://dx.doi.org/10.2174/1874067701406010001
4. G. Satyamaiah, M. Prasad, *Ind. J. Advance in chemical science*, 2014, 2(2),116.
5. D. T. Tayade, A. M. Kshirsagar, *Der chemica sinica*, 2013,4(4), 25.
6. M. I. Aralaguppi, T. M. Aminabhavi, *J Phys Chem*, 1991, 95, 5299. https://doi.org/10.1021/j100166a070
7. A. S. Burghate, P. B. Agrawal, M. L. Narwade, *Asian J. Chem*, 2001, 13(4), 1652.
8. S. D. Devsarkar, V. V. Pandhare, P. S. Kattekar, *J. Engineering*, 2012, 2013,1.
9. S. S. Dhondge, *J. Chem. Eng. Data*, 2010, 55, 3962. https://doi.org/10.1021/je901072c
10. G. B. Pethe, A. A. Ramteke, *J. Chem. Pharm*., 2010, 2(4), 68.
11. S. P. Wagh, Ph.D. *Thesis in Chemistry*, Amravati University, Amravati, (2004)
12. S. D. Deosarkar, M. L. Narwade, *Orin. J. Chem*., 2008, 24 (3), 1135.
13. U. P. Meshram, B. G. Khobragade, M. L. Narwade, *J. Chem. Pharm*, 2011, 3(3), 77. https://www.scopus.com/inward/record.uri?eid=2-s2.0-79957883279&partnerID=40&md5=ad2036d2049b5b9742fb14b00a202909
14. Anwar Ali, Rajan Patel, *J. Ind. chem. soc*., 2012, 89,1335.
15. Sajeevan Gaikwad, Suryavanshi Venkat, *JOCPR*, 2012, 4(3), 1851.
16. A N. Sonar, *European journal of biomedical and pharmaceutical sciences*, 2016, Volume 3, Issue 5, 345-347.
17. Pacak P; Kodejs Z., *Can. J. Chem*., 1988, 66, 2244 , https://doi.org/10.1139/v88-356
18. M.J. Iqbal; *M.A.* Chaudhry *J. Chem. Thermodynamics*, 2009, 41, 221-226, https://doi.org/10.1016/j.jct.2008.09.016

19. I. Banik, M.N. Roy, *J. Mol. Liq.*, 2012, 169, 8-14, https://doi.org/10.1016/j.molliq.2012.03.006.
20. R. Belda; J.V. Herraez, O. Diez, *Phys. Chem. Liq.*, 2005, 43, 91-101, https://doi.org/10.1080/00319100512331327342
21. D.J. Abraham, *Burgers medicinal chemistry and drug discovery, John-Wiley and Sons, Inc., Publications*, 6th Edn. Vol. 1, 2003,
22. Vogel A. I., *Practical Organic Chemistry*, 3 rd Edition, Longman, 1974,171.

Energy and Environment Focus
Vol. 7, pp. 1–8, 2022
www.aspbs.com/efocus

ARTICLE

Nanocubes SnO_2 Thin Films for the Detection of CO Gas

M. M. Patil and P. V. Dalal*

Nanocubes SnO_2 thin films have been prepared by spray pyrolysis method, under optimized conditions. The as prepared thin films were investigated by using X-ray diffraction, Field emission scanning electron microscope, Energy dispersive X-ray analysis, Transmission electron microscopy and Surface area electron diffraction pattern to know crystal structure, surface morphology, constituents of the elements and microstructure properties. The gas sensing performance was studied as a function of operating temperature. CO gas detection was also investigated with stability of thin films were studied and discussed.

Keywords: Spray Pyrolysis, Nanocubes SnO_2, CO Gas Sensing, Quick Response, Fast Recovery.

1. INTRODUCTION

Nanocubes SnO_2 is a versatile material having applications in the areas like transparent electrodes in photoelectric conversion devices namely amorphous silicon solar cells, liquid crystal display, gas sensor and many more [1–3], mainly due to their outstanding performance. Gas sensor have a great influence in many areas such as environmental monitoring, domestic safety, public over other possible materials such as SnO_2, TiO_2, WO_3, ZnO, In_2O_3, NiO due to its unique combination of interesting properties: non-toxicity, good electrical, optical and piezoelectric behavior and its low price.

The sensitivity of nanocubes SnO_2 gas elements is relatively high and is related to the grain size effect [4–7]. Some dangerous and poisonous gases, e.g., hydrogen, carbon monoxide, methane, LPG, ethanol etc. need to be detected, particular attention has been devoted to the monitoring of carbon monoxide (CO) [8].

For the purpose of control and safe applications in domestic and industrial field and in order to improve the gas sensing properties of the sensors, nature of the grains plays and important role in addtition, spray pyrolysis opens up the possibility to control the film morphology and particle size in nanometer range. Spray pyrolysis is a versatile technique for deposition of metal oxides [9].

Nanomaterials Research Laboratory, Department of Physics, Shri. V. S. Naik, Arts, Commerce and Science College, Raver, Jalgaon 425508, (M.S.) India

*Author to whom correspondence should be addressed.
Email: mmpatil1964@gmail.com
Received: 12 September 2021
Accepted: 25 April 2022

In the present investigations, nanocubes SnO_2 thin films were prepared by spray pyrolysis technique. Phase purity, morphology, composition of the elements and microstructure properties of thin films were studied using different analytical techniques. These nanocubes SnO_2 were tested for detection of different gases and were observed to be most sensitive to CO at 350 °C.

2. EXPERIMENTAL DETAILS

2.1. Preparation of Nanocubes SnO_2 Thin Films

Nanocubes SnO_2 thin films were prepared from aqueous solution of tin (II) dichloride dehydrate ($SnCl_2 \cdot 2H_2O$), Purified Merck) dissolved in deionized water to a concentration of 0.05 M for the preparation of thin films. The spray produced by nozzle was sprayed onto the ultrasonically cleaned glass substrates heated at 300 ± 5 °C. The deposition parameters like spray rate 5 mL/min. was adjusted using air as a carrier gas, nozzle to substrate distance (25 cm) were kept constant, and to and fro frequency of the nozzle (18 cycles min^{-1}) were kept constant at the optimized values indicated in brackets. Due to the air pressure of the carrier gas, a vacuum is created at the tip of the nozzle to suck the solution from the tube after which the spray starts. The precursor solution was sprayed on to the substrate in the air as small drops and around a high temperature zone where thermal decomposition and possible reaction between solutions occur, through compressed air, which is used as carrier gas with a flow rate controlled through air compressor regulator.

Various parameters such as nozzle-to-substrate distance, deposition time and flow rate of solution, deposition

Table I. Measurement of various parameters using different techniques.

Measuring techniques	Observations	D1	D2	D3	D4
Spray pyrolysis technique	Volume of sprayed solution (ml)	5	10	20	30
Surface profiler	Film thickness (nm)	556	768	873	943
Static gas sensing system	Activation energy (meV)	3.1	2.9	2.4	2.2
XRD	Crystallite size (nm)	12	14	16	17
FESEM	Average grain size (nm)	23	25	28	31

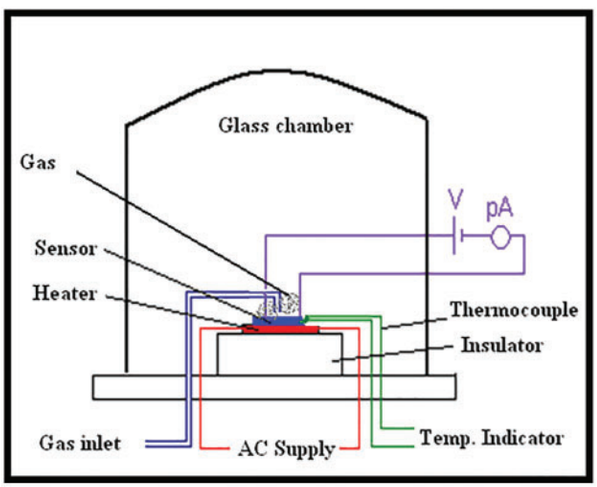

Fig. 1. Block diagram of gas sensing system.

temperature and concentration were optimized to get good quality films were tabulated in Table I. As the prepared nanocubes SnO_2 thin film samples D1, D2, D3 and D4 were annealed in air at 500 °C for 1 hour.

2.2. Sensing System to Test the Gases

Figure 1 shows block diagram of gas sensing system. The gas sensing studies were carried out using a static gas chamber to sense CO gas in air ambient. The nanocubes SnO_2 thin films were used as the sensing elements. Cr–Al thermocouple is mounted to measure the temperature. The output of thermocouple is connected to temperature indicator. Gas inlet valve fitted at one of the ports of base plate [9, 10].

Gas inlet valve fitted at one of the ports of the base plate. Gas concentration inside the static system is achieved by injecting a known volume of test gas in gas injecting syringe. Constant voltage is applied to the sensor and current can be measured by picoammeter.

3. CHARACTERIZATIONS OF THIN FILMS

3.1. Determination of Film Thickness

The thickness of thin films was measured by using Surface Profiler (AMBIOS Tech. (USA) XP.I) having a vertical resolution of 1.5 Å, lateral resolution of 100 nm and lateral length of 200 nm [11]. Thicknesses of nanocube SnO_2 thin film sample were in the range of 556 to 943 nm respectively.

3.2. Phase Studies Using X-ray Diffraction

The pure SnO_2 thin film were characterized by X-ray diffraction (Miniflex Model, Rigaku, Japan) using CuKα radiation with a wavelength, $\lambda = 1 \cdot 5418$ Å.

Figure 2 shows the X-ray diffractogram of thin film samples D1, D2, D3 and D4. The peaks in the XRD pattern are match well with the reported ASTM data of pure SnO_2 [9]. The average crystallite size of SnO_2 thin film samples were determined from the Scherrer formula [12]. The crystallite size was found to be increased from 12 to 17 nm with increase in the volume of the precursor solution from 5 to 30 ml respectively. Moreover it is found that crystallite size of SnO_2 film increases with increase in the volume of the precursor's solution due to the growth of crystallites.

$$D = 0 \cdot 9\lambda/\beta \cos\theta \tag{1}$$

Where, D = Average crystallite size; λ = X-ray wavelength ($1 \cdot 542$ Å); β = FWHM of the peak; θ = Diffraction peak position.

Without any impurity phase, indicating formation of single phase of SnO_2 strucure. It is revealed from X-ray diffractogram, the material is crystalline in nature with tetragonal phase.

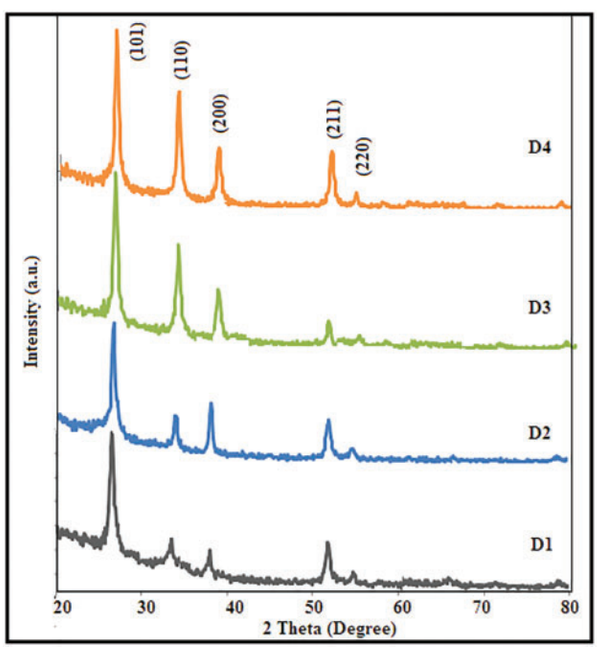

Fig. 2. X-ray diffractogram of SnO_2 thin films samples: D1, D2, D3 and D4.

3.3. Surface Morphology Using FESEM

The morphology of the films was analyzed using a field emission scanning electron microscope (FE-SEM, JEOL. JED 6300) coupled with EDAX.

Figures 3(D1)–(D4) shows the FESEM images, showing surface topography of D1, D2, D3 and D4 thin film samples respectively. Uniform and evenly distributed growth of SnO_2 nano crystals with cubic shape were observed. The estimated grain sizes were found to be in the range of 23 nm–31 nm. The grain size is found to increase with increase in volume of the precursor solution.

3.4. Quantitative Element Analysis (EDAX)

The elemental compositional study of the nanocubes SnO_2 were carried out by using the EDAX spectra. Figures 4(a)–(d) shows EDAX spectrum of the nanocubes SnO_2 thin films, which corroborates the presence of Sn and O in the sample.

Theoretically expected stoichiometric composition of SnO_2 (in terms of at.%) is: Sn = 33.33% and O = 66.66%. However, we actually obtained from EDAX the Sn and O content in the films were shown in the inset of Figures 4(a)–(d). It is clear from Table (Inset in Figs. 4(a–d)) that the sample D1 nearly stoichiometric and sample D2–D4 were nonstoichiometric in nature.

3.5. Microstructure Analysis Using TEM and Electron Diffraction Pattern

Microstructure property was studied using transmission electron microscopy (TEM, TECNAI G220 –TWIN FET, NETHERLAND: CM 200 Philips 200 kV HT).

In Figure 5(a) particle are seems to be cubic on the surface. Figure 5(b) shows the SAED image of the D3 sample indicates high crystallanity. TEM images confirms the nanocrystalline and cubic nature of the films. Low resolution of TEM image confirm that cubic nanostructure with uniform shape and particle size of about 90 nm were produced, in good agreement with the FESEM results.

4. ELECTRICAL PROPERTIES

4.1. I–V Characteristics

Figure 6 shows the I–V characteristics of samples D1, D2, D3 and D4 observed to be nearly symmetrical in nature indicating ohmic nature of contacts. The non-linear I–V characteristics may be due to semiconducting nature of the films [12].

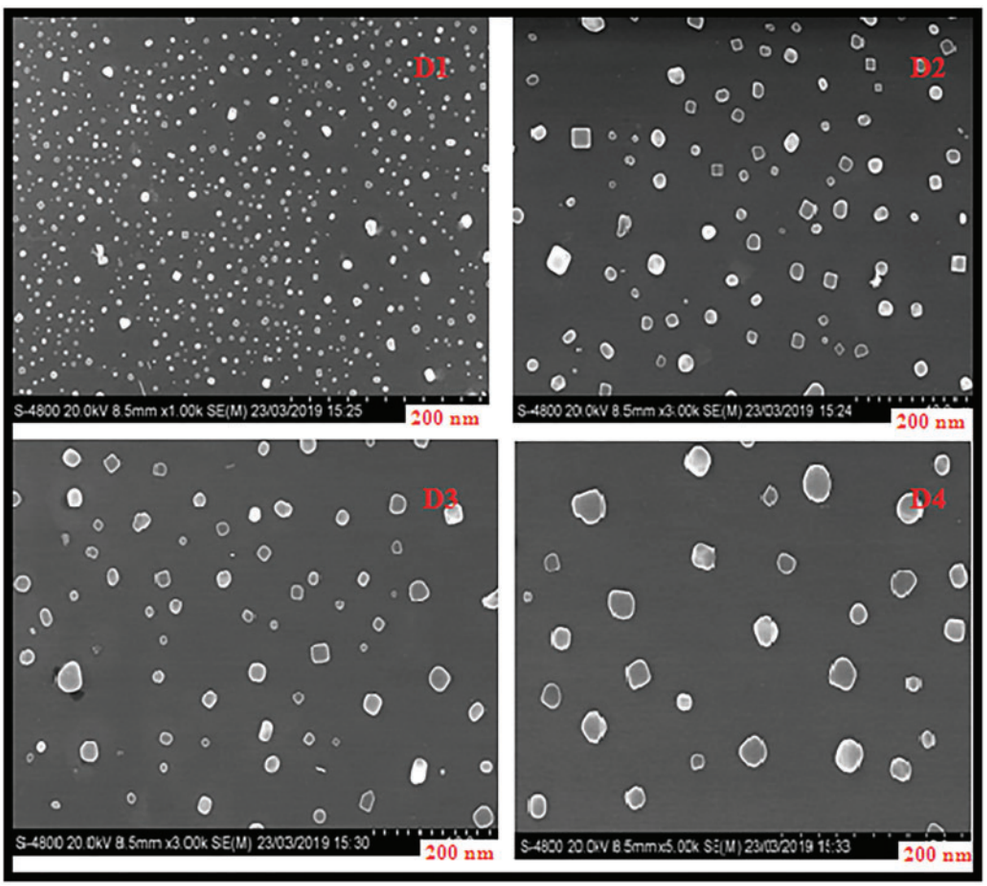

Fig. 3. FESEM images of nanocubes SnO_2 thin films samples: D1, D2, D3 and D4.

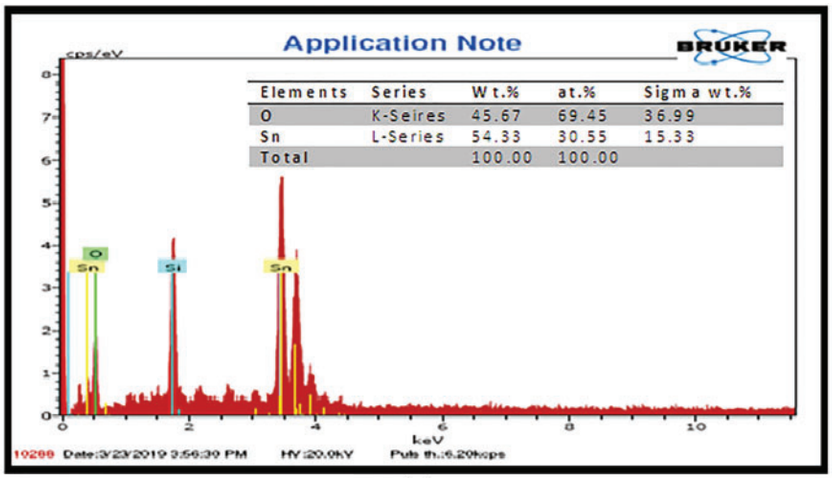

(a)

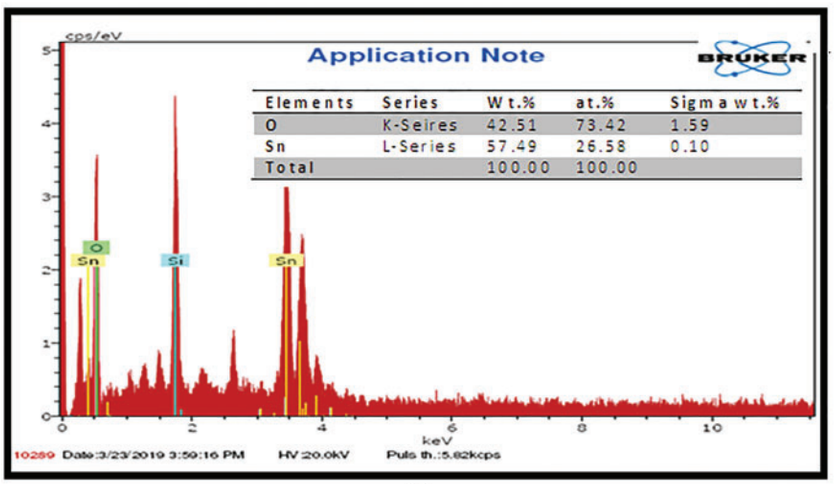

(b)

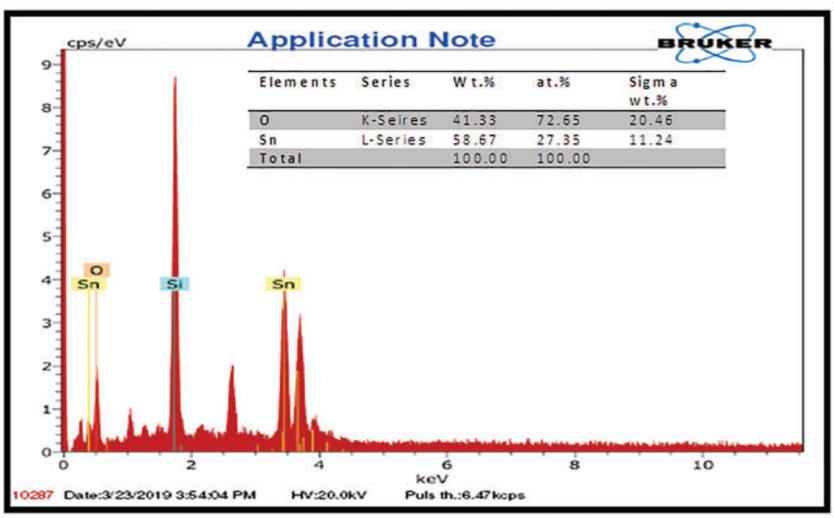

(c)

Fig. 4. Continued.

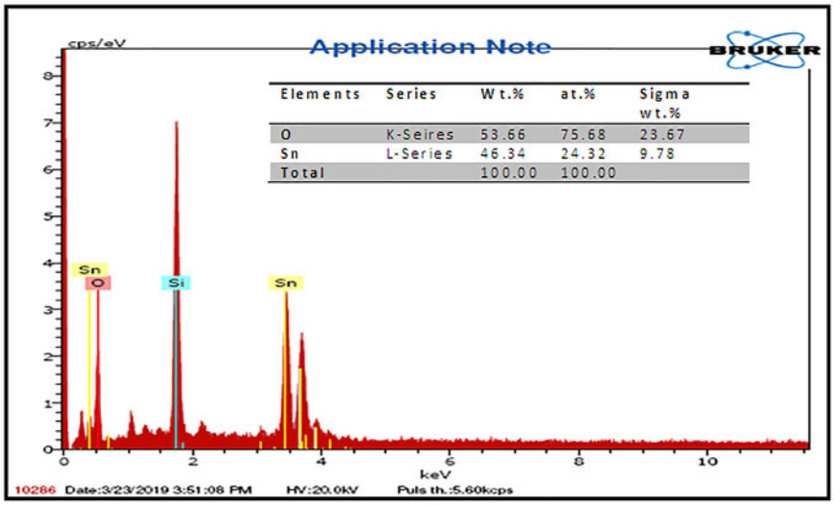

Fig. 4. (a–d) EDAX spectra of SnO_2 thin film samples: D1, D2, D3 and D4.

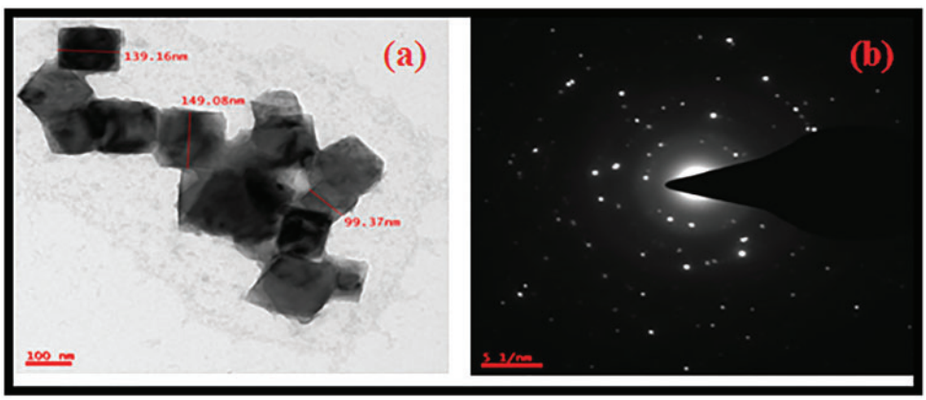

Fig. 5. (a–b) Represents the TEM and SAED image of the most sensitive sample N3.

4.2. Electrical Conductivity

Figure 7 show the variation of log (σ) with operating temperature. The conductivity of each sample is observed to be increasing with an increase in temperature range between 200 °C and 400 °C in steps of 50 °C. The increase in conductivity with increase in temperature could be attributed to negative temperature coefficient of resistance and semiconducting nature of nanocubes SnO_2 thin films.

The activation energies (ΔE) were calculated using the Arrhenius relation:

$$\sigma = \sigma_o \exp(-\Delta E/kT) \tag{2}$$

Where, σ = conductivity; σ_o = conductivity constant; k = Boltzmann constant; T = Temperature.

The activation energies were calculated from the slope of the graphs of logarithm of conductivity verses inverse of temperature and is found to be in the range of 3.1 meV to 2.2 meV.

The thickness of the film was varied from 556 to 943 nm. From Table I it was found that, as volume of sprayed solution increases, thickness of the films, crystallite size and grain size goes on increases while activation energy decreases. Such behavior could be due to the change in crystallite size and grain size accompanied with volume of sprayed solution. As well as probably due to the enhancement in the degree of crystallite of deposited film due to the increasing in grain size [13–16].

It is clear from Table I that, as film thickness of the sample goes on increasing; the activation energy goes on decreasing. The decrease in activation energy with increasing film thickness may be due to the change in structural parameters, improvement in crystalline and grain size [17].

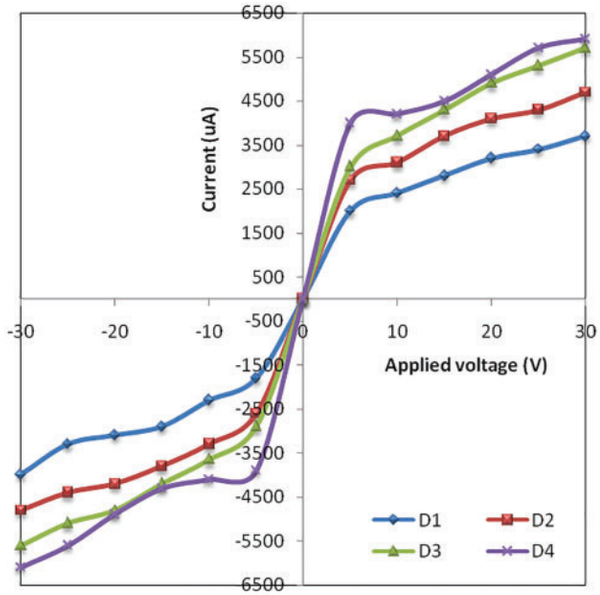

Fig. 6. I–V characteristics of nanocubes SnO_2 thin films.

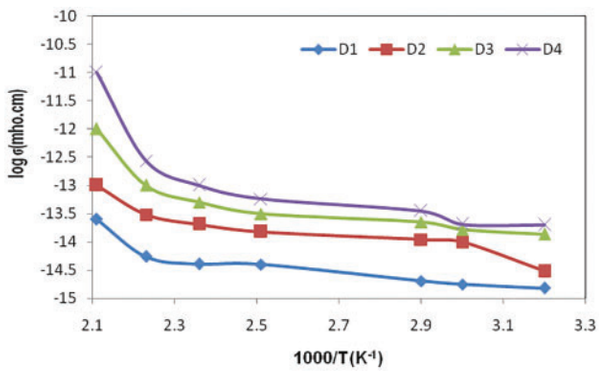

Fig. 7. Variation of log (σ) with operating temperature (°C).

5. GAS SENSING PERFORMANCE OF THE SENSORS

5.1. Gas Response

Figure 8 shows the variation in response with the operating temperature to 5 ppm of CO for D1, D2, D3 and D4

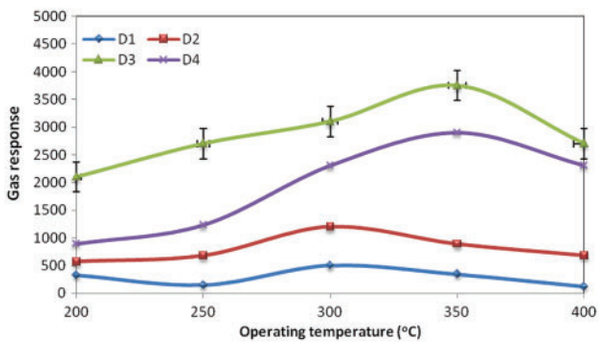

Fig. 8. Gas response of nanocubes SnO_2 thin films with operating temperature.

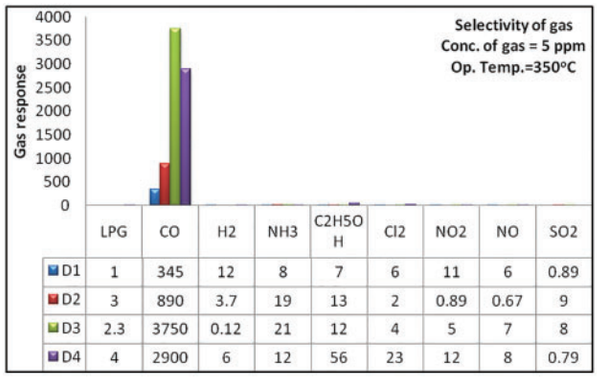

	LPG	CO	H2	NH3	C2H5OH	Cl2	NO2	NO	SO2
D1	1	345	12	8	7	6	11	6	0.89
D2	3	890	3.7	19	13	2	0.89	0.67	9
D3	2.3	3750	0.12	21	12	4	5	7	8
D4	4	2900	6	12	56	23	12	8	0.79

Fig. 9. Selectivity of nanocubes SnO_2 thin films for different gases.

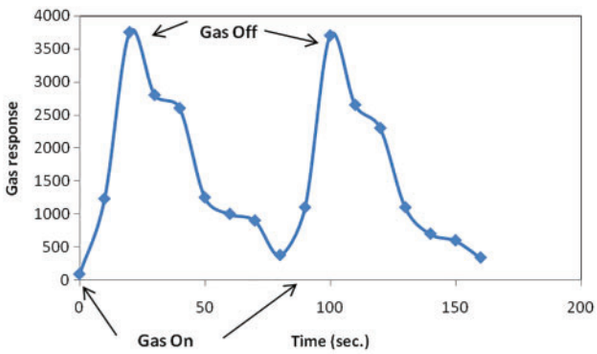

Fig. 10. Response and recovery of the sensor.

samples. For all the samples the response increases with increase in operating temperature and reach maximum (S = 3750 for sample D3) at 350 °C and falls with further increase in operating temperature. Thus, in the present case the optimum operating temperature for nanocubes SnO_2 films was 350 °C. The temperature, which corresponds to a certain peak value, is a function of the kind of target gases and the chemical composition of the oxide, including additives and catalysts, and pure oxides are generally stable at lower temperatures [18].

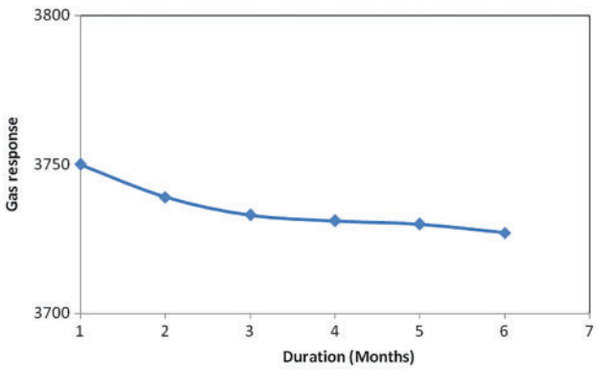

Fig. 11. Stability profile of the most sensitive sample D3.

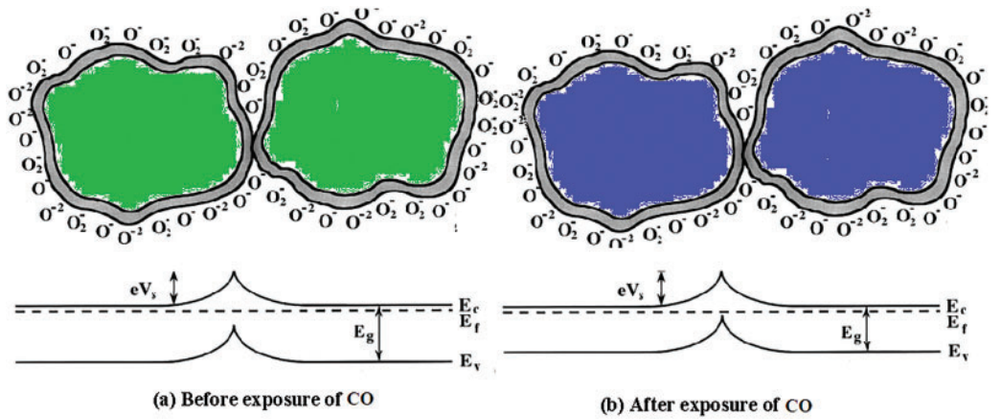

Fig. 12. Gas sensing mechanism of thin film.

For the sample D4 gas response decrease due to the enhancement in grain size of the cubes [19]. From the FESEM images it is found that as volume of the precursor solution increases the network of cubes seem to expand due to lack of cohesion among the film particles (Table I).

5.2. Selectivity

Figure 9 shows the histogram for comparison of the sensitivity to various gases for D1, D2, D3 and D4 at the optimum operating temperature 350 °C. The table attached to histogram shows the sensitivity values, it is clear that the S3 film is highly selective to CO (5 ppm) against all other tested gases: LPG, H_2, NH_3, C_2H_5OH, Cl_2, NO_2, NO and SO_2.

5.3. Response and Recovery of the Sensor

The response and recovery of the nanocubes SnO_2 most sensitive thin film (D3) sensor on exposure of 5 ppm of CO_2 at 350 °C are represented in Figure 10. The response is quick (30 s) and recovery is fast (60 s). The high oxidizing ability of adsorbed oxygen species on the surface nanoparticles and high volatility of desorbed by-products explain the quick response to CO gas and fast recovery [20, 21].

5.4. Stability of Sensor

The stability of the nanocubes SnO_2 most sensitive thin film (D3) was measured by repeating the test many times (6 Month). From Figure 11 it is observed that the nanocubes SnO_2 thin film response is stable for gas sensing application. During the test, slightly variation was observed in gas response as shown in Figure 11.

6. GAS SENSING MECHANISM

It has been known that the gas-sensing mechanism of SnO_2 gas sensor is primary ascribed to the resistance change of SnO_2 in different target gas atmospheres, which is caused by the adsorption and desorption of target gas molecules on the surface of SnO_2. In air atmosphere, oxygen molecules are adsorbed on the surface of SnO_2 and capture the electrons from the conduction band of SnO_2 [22, 23].

Under this condition, the concentration of free electrons in the conduction band of SnO_2 decreased (shown in Figs. 12(a and b)), forming the electron depletion layer and potential barrier on the surface and at grain boundaries, respectively.

Firstly, the incorporation of CO gas into SnO_2 resulted in rich surface oxygen vacancies. These surface oxygen vacancies tend to adsorb oxygen molecules, because of the lower adsorption energy of oxygen molecules on the oxygen vacancy sites than that on the perfect sites.

Therefore, these surface oxygen vacancies can act as electron donors, making a great quantity of electrons in the conductive band captured in air and released in acetone atmosphere. It would greatly increase the difference of the width of depletion layer and the height of potential barrier in different atmospheres, resulting in a higher response [24, 25].

Secondly, the incorporation of CO gas into SnO_2 resulted in the reduction of particle size, along with the large surface area and unique cubic structure. These would provide more active sites on the surface of SnO_2, and facilitate acetone diffusion and mass transport within sensing material. Therefore, the nanocubes SnO_2 shows a superior gas sensing property [26].

7. CONCLUSIONS

(1) Nanocubes SnO_2 thin films could be prepared by simple and inexpensive spray pyrolysis technique.
(2) The structural, morphological and microstructural properties confirm that the as-prepared SnO_2 thin films are nanostructured in nature.
(3) The EDAX data indicated that thin films samples were nonstoichiometric in nature.

(4) Thickness of the films was observed to increase from 556 nm to 943 nm with increase in volume of the sprayed solution.
(5) Crystallite size and gain size were increases with increase in film thickness.
(6) The Nanocubes SnO_2 thin film of sample D3 = 3750 was most sensitive to CO gas to the gas concentration as 5 ppm at the temperature of 350 °C.
(7) The sensor has good selectivity to CO against different gases.
(8) The nanocubes SnO_2 thin films exhibit rapid response-recovery with good stability which is one of the main features of this sensor.

Acknowledgments: The authors are thankful to The Principal, Shri. V. S. Naik Arts, Commerce and Science College, Raver for providing necessary laboratory facilities for this work.

References and Notes

1. Mirzaei, A., Leonardi, S.G. and Neri, G., **2016**. Detection of hazardous volatile organic compounds (VOCs) by metal oxide nanostructures-based gas sensors: A review. *Ceramics International*, *122*(42), pp.15119–15141.
2. Gupta, P. and Sharma, S.K., **2017**. A study of oxygen gas sensing in Zn-doped SnO_2 nanostructures. *Materials Research Express*, *34*(4), pp.065010–065018.
3. Hsueh, T.-J. and Lub, C.-L., **2019**. A hybrid YSZ/SnO_2/MEMS SO_2 gas sensor. *Royal Society of Chemistry*, *9*, pp.27800–27806.
4. Zhao, Y., Duan, L., Xing, J., Larssen, T., Nielsen, C.P. and Hao, J.M., **2009**. Soil acidification in China: Is controlling SO_2 emissions enough. *Environmental Science and Technology*, *43*, pp.8021–8026.
5. Schwandta, C., Kumara, R.V. and Hills, M.P., **2018**. Solid state electrochemical gas sensor for the quantitative determination of carbon dioxide. *Sensors and Actuators, B*, *265*, pp.27–34.
6. Antunes, F.C., Goulart, C.A., Andreeta, M.R.B. and de Souza, D.P.F., **2018**. YSZ/Al_2O_3 multilayer thick films deposited by spin coating using ceramic suspensions on Al_2O_3 polycrystalline substrate. *Mater. Sci. Eng., B*, *228*, pp.60–66.
7. Mitra, P., Chatterjee, A.P. and Maiti, H.S., **1998**. ZnO thin film sensor. *Materials Letters*, *35*, pp.33–38.
8. Betty, C.A. and Choudhury, S., **2016**. Charge carrier transport in nanocrystalline SnO_2 thin film sensor and temperature dependence of toxic gas sensitivity. *Sensors and Actuators, B*, *237*, pp.787–794.
9. Chang, S.J., Hsueh, T.J., Chen, I.-C. and Huang, B.R., **2008**. Highly sensitive ZnO nanowire CO sensors with the adsorption of Au nanoparticles. *Nanotechnology*, *19*, pp.175502–175506.
10. Cirera, A., Vila, A., Diéguez, A., Cabot, A., Corne, A. and Morante, J.R., **2000**. Microwave processing for the low cost, mass production of undoped and in situ catalytic doped nanosized SnO_2 gas sensor powders. *Sensors and Actuators, B*, *64*, pp.65–69.
11. Duan, Z., Zhang, Y., Tong, Y., Zou, H., Peng, J. and Zheng, X., **2017**. Mixed-potential-type gas sensors based on Pt/YSZ film/$LaFeO_3$ for detecting NO_2. *Journal of Electronic Materials*, *46*, pp.6895–6900.
12. Lu, C.L., Changa, S.J., Weng, T.C. and Hsueh, T.J., **2018**. A bifacial SnO_2 thin film ethanol Gas sensor. *IEEE Electron Device Lett.*, *39*, pp.1223–1225.
13. Kou, X., Xie, N., Chen, F., Wang, T., Guo, L., Wang, Ch., Wang, Q., Ma, J., Sun, Y., Zhang, H. and Lu, G., **2018**. Superior acetone gas sensor based on electrospun SnO_2 nanofibers by Rh doping. *Sensors and Actuators, B*, *256*, pp.861–869.
14. Xing, R., Xu, L., Song, J., Zhou, C., Li, Q., Liu, D. and Song, H.W., **2015**. Preparation and gas sensing properties of In_2O_3/Au nanorods for detection of volatile organic compounds in exhaled breath. *Scientific Reports*, *5*(10717), pp.1–14.
15. Wei, S., Zhao, G., Du, W. and Tian, Q., **2016**. Synthesis and excellent acetone sensing properties of porous WO_3 nanofibers. *Vacuum*, *124*, pp.32–39.
16. Narjinary, M., Rana, P., Sen, A. and Pal, M., **2017**. Enhanced and selective acetone sensing properties of SnO_2-MWCNT nanocomposites: Promising materials for diabetes sensor. *Materials and Design*, *115*, pp.158–164.
17. Salehi, S., Nikan, E., Khodadadi, A.A. and Mortazavi, Y., **2014**. Highly sensitive carbon nanotubes-SnO_2 nanocomposite sensor for acetone detection in diabetes mellitus breath. *Sensors and Actuators, B*, *205*, pp.261–267.
18. Kalidoss, R., Umapathy, S. and Sivalingam, Y., **2018**. An investigation of GO-SnO_2–TiO_2 ternary nanocomposite for the detection of acetone in diabetes mellitus patient's breath. *Applied Surface Science*, *449*, pp.677–684.
19. Zhang, Z., Xu, M., Liu, L., Ruan, X., Yan, J., Zhao, W., Yun, J., Wang, Y., Qin, S. and Zhang, T., **2018**. Novel SnO_2–ZnO hierarchical nanostructures for highly sensitive and selective NO_2 gas sensing. *Sensors and Actuators, B*, *257*, pp.714–727.
20. Lee, I., Choi, S.J., Park, K.M., Lee, S.S., Choi, S., Kim, I.D. and Park, C.O., **2014**. The stability, sensitivity and response transients of ZnO, SnO_2 and WO_3 sensors under acetone, toluene and H_2S environments. *Sensors and Actuators, B*, *197*, pp.300–307.
21. Perillo, P.M., **2016**. Flexible gas sensor based on TiO_2 membrane nanotubes for detection of butylamine. *Mater. Today. Commun.*, *7*, pp.117–121.
22. Karthik, T.V.K., Martinez, L. and Agarwal, V., **2018**. Porous silicon ZnO/SnO_2 structures for CO_2 detection. *J. Alloy Compd.*, *731*, pp.853–863.
23. Bari, R.H., Patil, S.B., Baril, A.R., Patil, G.E. and Aambekar, J., **2012**. Spray pyrolysed nanostructured ZnO thin film sensors for ethanol Gas. *Sensors & Transducers Journal*, *140*(5), pp.124–132.
24. Janotti, A. and Van, G., **2009**. Fundamentals of zinc oxide as a semiconductor. *Reports on Progress in Physics*, *72*, pp.1–29.
25. Song, X., Wang, Z., Liu, Y., Wang, C. and Li, L., **2009**. A highly sensitive ethanol sensor based on mesoporous ZnO–SnO_2 nanofibers. *Nanotechnology*, *20*, pp.1–5.
26. Yan, S.H., Ma, S.Y., Li, W.Q., Xu, X.L., Cheng, L., Song, H.S. and Liang, X.Y., **2015**. Synthesis of SnO_2–ZnO heterostructured nanofibers for enhanced ethanol gas-sensing performance. *Sensors and Actuators, B*, *221*, pp.88–95.